Quantum Mechanical Interpretation of Nitrite Reduction by Cytochrome cd_1 Nitrite Reductase from *Paracoccus pantotrophus*†

Graziella Ranghino,*,‡ Erminia Scorza,‡ Tove Sjögren,§ Pamela A. Williams,|| Marco Ricci,‡ and Janos Hajdu*,§

EniChem S.p.A., Via G. Fauser n. 4, I-28100 Novara, Italy, Department of Biochemistry, Uppsala University, Box 576, S-751 23 Uppsala, Sweden, and Department of Molecular Biology, The Scripps Research Institute, 10550 North Torrey Pines Road, La Jolla, California 92037

Received January 31, 2000; Revised Manuscript Received June 26, 2000

ABSTRACT: The reduction of nitrite to nitric oxide in respiratory denitrification is catalyzed by a cytochrome cd_1 nitrite reductase in *Paracoccus pantotrophus* (formerly known as *Thiosphaera pantotropha* LMD 92.63). High-resolution structures are available for the fully oxidized [Fülöp, V., Moir, J. W., Ferguson, S. J., and Hajdu, J. (1995) *Cell 81*, 369−377; Baker, S. C., Saunders, N. F., Willis, A. C., Ferguson, S. J., Hajdu, J., and Fülöp, V. (1997) *J. Mol. Biol. 269*, 440−455] and fully reduced forms of this enzyme, as well as for various intermediates in its catalytic cycle [Williams, P. A., Fülöp, V., Garman, E. F., Saunders, N. F., Ferguson, S. J., and Hajdu, J. (1997) *Nature 389*, 406−412]. On the basis of these structures, quantum mechanical techniques (QM), including density functional methods (DFT), were combined with simulated annealing (SA) and molecular mechanics techniques (MM) to calculate the electronic distribution of molecular orbitals in the active site during catalysis. The results show likely trajectories for electrons, protons, substrates, and products in the process of nitrite reduction, and offer an interpretation of the reaction mechanism. The calculations indicate that the redox state of the d_1 heme and charges on two histidines in the active site orchestrate catalysis locally. Binding of nitrite to the reduced iron is followed by proton transfer from His345 and His388 to one of the oxygens of nitrite, creating a water molecule and an [Fe(II)-NO^+] complex. Valence isomerization within this complex gives [Fe(III)-NO]. The release of NO from the ferric iron is influenced by the protonation state of His345 and His388, and by the orientation of NO on the d_1 heme. Return of Tyr25 to a hydrogen-bonding position between His345 and His388 facilitates product release, but a rebinding of Tyr25 to the oxidized iron may be bypassed in steady-state catalysis.

Three-dimensional X-ray movies on catalysis and ligand binding have opened up new possibilities in structural biology. The combination of X-ray diffraction with single-crystal spectrophotometry allows the correlation of electronic transitions with structural transitions in crystals of macromolecules (*3*−*7*). Mechanistic interpretation of the data can be further enhanced by quantum chemical techniques, and in this paper, we describe results from quantum and molecular mechanics calculations on likely trajectories for electrons, protons, substrates, and products during nitrite reduction in crystals of cytochrome cd_1 nitrite reductase from *Paracoccus pantotrophus*. The calculations are based on the known high-resolution crystal structures of the oxidized (*1*, *2*) and reduced forms of the enzyme (*3*) as well as on structures of key reaction intermediates trapped in time-resolved experiments during nitrite reduction (*3*).

Cytochrome cd_1 nitrite reductase from *P. pantotrophus* is a soluble dimeric hemoprotein (*8*), which under physiological conditions catalyzes the reduction of nitrite to nitric oxide in respiratory denitrification (for reviews, see refs *9* and *10*). The enzyme can also catalyze the four-electron reduction of oxygen to water, and has thus also been known as a soluble cytochrome oxidase. The two chemically identical subunits of the protein are organized into two domains (*1*, *2*). Residues 1−134 form a *c*-type cytochrome domain, containing a *c* heme attached to residues Cys65 and Cys68, while residues 135−567 form a rigid C-terminal β-propeller domain, containing the d_1 heme in the core of an eight-bladed β-propeller structure. The *c* heme is the site of entry for electrons from external donors (*11*), while the d_1 heme is the site of nitrite and oxygen reduction. The distal coordination geometry of the d_1 heme in oxidized crystals of the enzyme is different in different species (*1*, *12*−*14*). Other residues (e.g., His200, His345, and His388) are conserved in the active site.

A fascinating feature of nitrite reduction by cytochrome cd_1 is that nitric oxide is formed on the iron of the d_1 heme from where it must leave as a reaction product despite its considerable affinity for the heme iron. In an attempt to identify key steps in nitrite reduction by cytochromes cd_1, in this paper we use quantum chemical techniques to examine

† Supported by the Swedish Natural Science Research Council and EU-BIOTECH (BIO4-CT96-0281 and BIO4-CT98-0415).

* To whom correspondence should be addressed. G.R.: EniChem S.p.A., Via G. Fauser n. 4, I-28100 Novara, Italy; e-mail, Graziella.Ranghino@enichem.it; fax, +39-0321-447425. J.H.: Department of Biochemistry, Uppsala University, Box 576, SE-751 23 Uppsala, Sweden; e-mail, janos@xray.bmc.uu.se; fax, +46-18-511755.

‡ EniChem S.p.A.

§ Uppsala University.

|| The Scripps Research Institute.

10.1021/bi000178y CCC: $19.00
Published on Web 08/12/2000

the stereoelectronic mechanism of nitrite reduction at a d_1 heme center, and consider the relevance of experimentally obtained crystal structures to the process of steady-state nitrite reduction.

Initial quantum mechanical simulations were performed in vacuo on stripped-down models of the active site to reduce the system to a computationally manageable size. This minimal system was subsequently extended to account for the effect of charges elsewhere in the protein and the effect of screening and solvation by the protein and its ordered solvent environment. These factors were taken into account by molecular mechanics calculations based on the known three-dimensional structures of these intermediates, and included the whole protein and all ordered solvent molecules identified in these structures.

METHODS

Models of the Active Site. Stripped-down models of the active site were derived from available X-ray structures, and in all cases included the d_1 heme, His200, His345, His388, Asp346, and a water molecule near His388 (cf. Figure 2). In addition, some models also contained a bound nitrite ion or nitric oxide molecule on the d_1 heme iron, and Tyr25 in or near the active site when it was seen in those positions in the X-ray structure. Hydrogen atoms were added, and their positions were energetically optimized, first by means of the molecular mechanics minimization option in the program package Cerius2 (Cerius2 3.0, MSI, San Diego, CA), followed by quantum mechanical energy minimization, using a variant of the Newton−Raphson minimization procedure (*15*) known as the BFGS or VA09A scheme to direct the system to the nearest local minimum on the energy surface.

Quantum Mechanical Energy Calculations. The density functional theory (DFT)[1] of Kohn and Sham (*16*) was used to determine the energy of the many-atom system. The energy was written as a function of the electron density according to Harris (*17*). In addition, the "local density approximation" (LDA) for the exchange and correlation term was used (*16*). The program uses a Gaussian-type atomic orbital basis set. The actual basis set included 956 basis functions, containing full cores for all light atoms (double Z for hydrogen, single Z for carbon, nitrogen, and oxygen). The basis set for iron contained five core functions and five valence functions. The radial cutoff for the integrals was 10 Å. The calculations used the FastStructure application of the CERIUS2 3.0 program package (Cerius2 3.0, MSI). Local exchange correlation potential was calculated by the method of Barth and Hedin (*18*). Energy differences were calculated between isoelectronic models, and when the difference was the protonation state, the energy of deprotonation was added to account for the contribution of deprotonation to the total energy of the different models with different numbers of protons. This was evaluated as the energy difference between the isolated charged and uncharged residues. The binding energies were computed with the equation $\Delta AB = E_{AB} - E_A - E_B$, where E_{AB} is the total energy of the complex and E_A and E_B are the total energies of the isolated components. This approach uses simple reference states (i.e., the isolated components). Other schemes may also be used. We note that the numerical outcome of the calculations is affected by the selection of the reference sets and by the influence of the protein and solvent environment surrounding the model (see Molecular Mechanics).

Simulated Annealing Procedures. Simulated annealing was used to establish likely links between structures in the reaction pathway. Simulated annealing also ensures that the system is directed to a low-lying minimum, and is not trapped in a high-lying local minimum as in the BFGS optimization above. The method of Kirkpatrick et al. (*19*) was used as implemented in the FastStructure program (Cerius2 3.0, MSI). A typical simulated annealing calculation consisted of a series of laps each characterized by a given temperature and a number of time steps. The basis set was the same as the one described above for the quantum mechanical energy calculations. The protocol for analyzing nitric oxide formation was the following: a starting temperature of 600 K and a final temperature of 200 K. This final temperature was reached in laps of 10 steps with the temperature decreasing by 50 K per lap with a total of 90 steps. Another 10 steps at the lowest temperature were added. In the case of the release of nitric oxide from the heme iron, the number of steps was set to 100 or 200 and the temperature was quenched from 600 to 200 K. The Cβ atoms of His200, His388, His345, and Asp346 were fixed as the crystal structures indicate no significant movements for these atoms during catalysis. All other atoms were allowed to shift their positions.

Molecular Mechanics. In the next step, the ab initio quantum mechanical models (described above) were incorporated into the whole protein to account for the effect of charges elsewhere and the effect of screening and solvation both by the protein and by its immediate solvent environment. The DISCOVER molecular dynamics program, from the INSIGHT-II program package (MSI), was used to perform structural minimization, optimization, and molecular dynamics calculations on the system. Hydrogen positions were optimized both on the protein and on the solvent molecules to achieve an energy minimum for the entire system (protein + solvent + correct hydrogen positions). Conditions for energy minimization of the protein were established by assigning charges based on the CVFF force field in INSIGHT. The two hemes were treated separately. Parameters for all atoms of the *c* heme, including the iron and the axial ligands, were assigned using an extended CVFF force field (*20*), while charges for the d_1 heme were derived from the ab initio calculations described above. The DOCKING option of INSIGHT-II was subsequently used to compute the interaction energies of nitric oxide and nitrite when bound to the d_1 heme in the extended environments. This approach takes into consideration the interaction of the ligand with the solvated protein as present in the crystal and defined in the PDB file.

RESULTS AND DISCUSSION

Figure 1 shows a scheme for nitrite reduction in cytochrome cd_1 nitrite reductase. Structures supported by X-ray data are highlighted by boxes in the figure, and Table 1 gives a summary of relevant crystallographic data for these

[1] Abbreviations: QM, quantum mechanics; SA, simulated annealing; DFT, density functional theory; MM, molecular mechanics; LDA, local density approximation; LUMO, lowest unoccupied molecular orbital; HOMO, highest occupied molecular orbital; SOMO, singly occupied molecular orbital; PDB, Protein Data Bank.

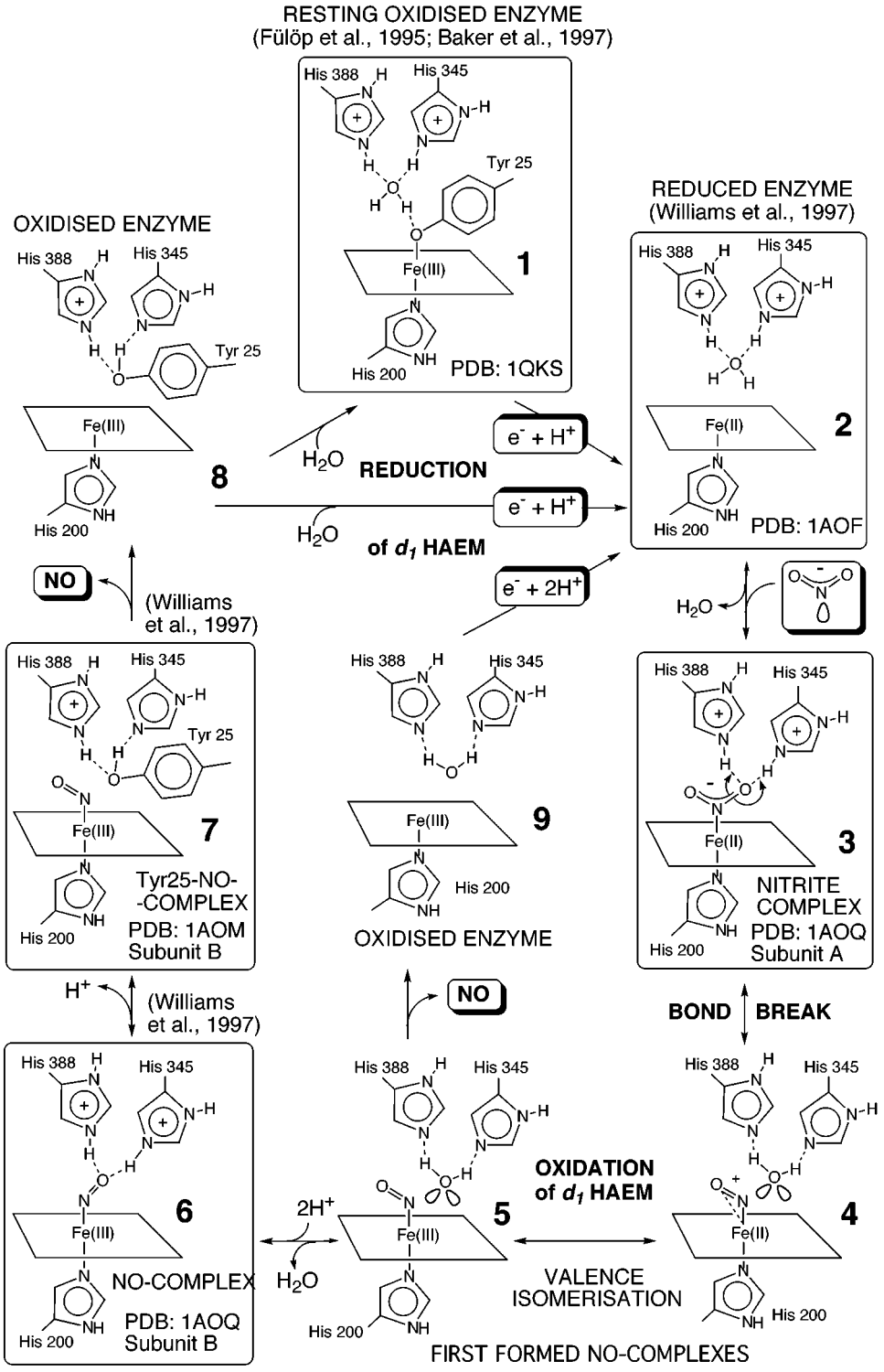

FIGURE 1: Possible routes for nitrite reduction in cytochrome cd_1 nitrite reductase from *P. pantotrophus* LMD 92.63. Boxes highlight structural forms for which X-ray structures exist (*1*−*3*, *21*). Most structures could be drawn in other isoelectronic forms in which the ionization states of His345 and His388 and their hydrogen-bonding patterns are different. His345 and His388 are conserved in cytochromes cd_1. Starting from the resting oxidized enzyme (structure **1**), nitrite reduction may proceed through three major routes: **1**, **2**, **3**, **4**, **5**, **6**, **7**, **8**, **1**; **1** → **2**, **3**, **4**, **5**, **9**, **2**; and **1** → **2**, **3**, **4**, **5**, **6**, **7**, **8**, **2**. At low nitrite concentrations and when the supply of reducing equivalents is low, the system returns to the fully oxidized resting form [structure **1** (*3*)].

structures. Involvement of other structures in catalysis has been inferred from available chemical data and from calculations described below. Structure **1** (Figure 1) represents the fully oxidized enzyme (*1*) for which a 1.29 Å structure has been published (*2*). Reduction of this form in the crystalline state produces structure **2** (*3*). In structure **2**, Tyr25 is no longer a ligand to the d_1 heme, enabling the substrate to bind in its place. Nitrite binds to the reduced d_1 heme iron [structure **3** (*3*)], and following the transfer of two protons (structures **3** and **4**) and one electron (structure **5**) to the substrate, a water molecule and a molecule of nitric oxide are produced. The enzyme may then return to structure **1**, and indeed, it does do so in the crystal when all reducing equivalents are used up (*3*).

Table 1: X-ray Structures[a] Used for Quantum Chemical Calculations

PDB code	description	structure in Figure 1	resolution (Å)	R_{cryst}/R_{free}	ref
1QKS	fully oxidized enzyme	**1**	1.28	18.5/20.0	*1* and *2*
1AOF	fully reduced enzyme	**2**	2.0	16.3/20.1	*3*
1AOQ	reduced enzyme and nitrite (**2**)	**3** and **6**	1.8	17.6/19.7	*3*
1AOM	reduced enzyme and nitrite (**1**)	**7**	1.8	18.1/20.0	*3*

[a] These structures appear in boxes in Figure 1.

While these changes could very clearly be observed in the crystal (*3*), consideration has been given to the possibility that the structure of the fully oxidized enzyme [structure **1** (*1*, *2*)] in which Tyr25 is bound to the d_1 heme represents a resting state of the protein (*3*, *12*, *21*, *22*). Pulse radiolysis studies on the electron transfer within cytochrome cd_1 from *P. pantotrophus* show evidence for a fast intramolecular electron transfer from the *c* heme to the d_1 heme (*23*). Such transfer speeds would be unlikely if a return to the resting state was an integral part of steady-state catalysis. Mutagenesis studies on the *Pseudomonas aeruginosa* enzyme show that the active site tyrosine in that enzyme is not necessary for catalysis (*24*). The amino acid sequence of the *Pseudomonas stutzeri* enzyme (*25*, *26*) indicates there is no tyrosine in the N-terminal domain of the *Ps. stutzeri* enzyme. These findings confirm that a rebinding of a tyrosine residue to the d_1 heme, and thus a return to the resting fully oxidized state, cannot be a mandatory part of the catalytic cycle in all cytochromes cd_1.

The Open Active Site in the Reduced Enzyme. Nitrite binds to the reduced form of the enzyme [structure **2**, Figure 1, PDB entry 1AOF (*3*)] in which the active site is open. One of the oxygens of the bound nitrite ion forms hydrogen bonds with His345 and His388 (Figure 2A, also shown schematically as structure **3** in Figure 1). His345 and His388 are conserved in cytochromes cd_1, and are believed to participate in the protonation of the substrate (*1*).

As a first step, we assess the effect of the charge states of these histidines on the thermodynamical stability of the open and unliganded active site prior to substrate binding. The model for the empty active site included all atoms of the d_1 heme, the axial histidine ligand (His200), residues His345, His388, and Asp346 above the heme plane, and two water molecules (for other details, see Methods).

Results of single-point energy calculations indicate that the most stable form of the open reduced enzyme is the form in which both His345 and His388 are protonated (Table 2). Under such conditions, the active site has a net positive charge, which could help in guiding the negatively charged substrate into the binding pocket through Coulombic interactions. The effect of the oxidation state of the d_1 heme on the stability of the unliganded active site was considered. A hypothetical model was created in which the ferrous iron was replaced with a ferric iron in the d_1 heme (shown schematically as structure **9**, in Figure 1, with unprotonated histidines). The energetically most favored form of the open ferric enzyme is the one in which His388 is protonated while His345 is not (Table 2). The distinction between the two histidines is due to the favorable interaction of Asp346 with His388, and this interaction could stabilize a positive charge on His388. This effect becomes prominent when an electron is removed from the d_1 heme, changing the overall charge state of the active site. The last column of Table 2 highlights differences in the total energy of the system when shielding or solvation is taken into account by using the CVFF modified force field of Angelucci et al. (*20*) in the molecular mechanics program DISCOVER (see Methods). The data show that the structure in which His388 is protonated is the most stable one followed by the doubly charged form (with both histidines protonated) and finally by the structure in which His354 is protonated.

Nitrite Binding. Two very similar structures have been published for the complex in which nitrite is bound to the reduced d_1 heme [PDB entries 1AOQ (subunit A) and 1AOM (subunit A) (*3*)]. These structures were obtained by flash-freezing reduced crystals after soaking them in a nitrite solution for a short period of time (60 or 180 s). Both structures show that one of the oxygens of the bound nitrite forms hydrogen bonds with His345 and His388 (Figure 2A, and structure **3** in Figure 1). Table 3 shows the thermodynamic stability of the enzyme−nitrite complex as a function of the protonation state of His345 and/or His388. The most stable structure for the ES complex is the one in which the iron is reduced and both His345 and His388 act as hydrogen bond donors to nitrite (Figure 2A). The last column of Table 3 shows docking energies obtained with DISCOVER (see Methods) when nitrite binds in the active site of the protein [1AOQ (subunit A)]. The most favorable case is when both histidines are protonated, which is also the most stable form according to the initial ab initio estimate. All available data indicate that the d_1 heme is reduced in such a complex. A simulated annealing experiment starting from oxidized iron in the d_1 heme produced a highly distorted heme ring. Such ring geometry was not observed in the X-ray experiments, and the enzyme−nitrite complex turns over to products in the crystal.

Formation of Nitric Oxide. Nitrite reduction on the d_1 heme produces a water molecule and leaves a molecule of nitric oxide bound to the iron. X-ray structures (*3*) for the product complex show bound NO in a bent conformation (ref *3* and structures **6** and **7** in Figure 1; also, see Figure 2C,D), and experimental evidence suggests the d_1 heme is oxidized (*3*). Quantum mechanical techniques combined with simulated annealing (see Methods) were used to mimic nitrite reduction. These simulations were started from the X-ray structure of the enzyme−nitrite complex (Figure 2A, or structure **3** in Figure 1). To facilitate water release and to simulate a vibrational mode, the N−O bond of nitrite was stretched by 0.2 Å in the starting model. The final structure calculated by simulated annealing shows two protons migrated from His345 and/or His388 to the oxygen of nitrite, and the oxygen was cleaved off in the form of a water molecule (Figure 2B). The d_1 heme contained a ferrous iron at this stage, and there was a formal positive charge on the bound nitric oxide (structure **4** in Figure 1). The product water molecule was a hydrogen bond donor to the two histidines.

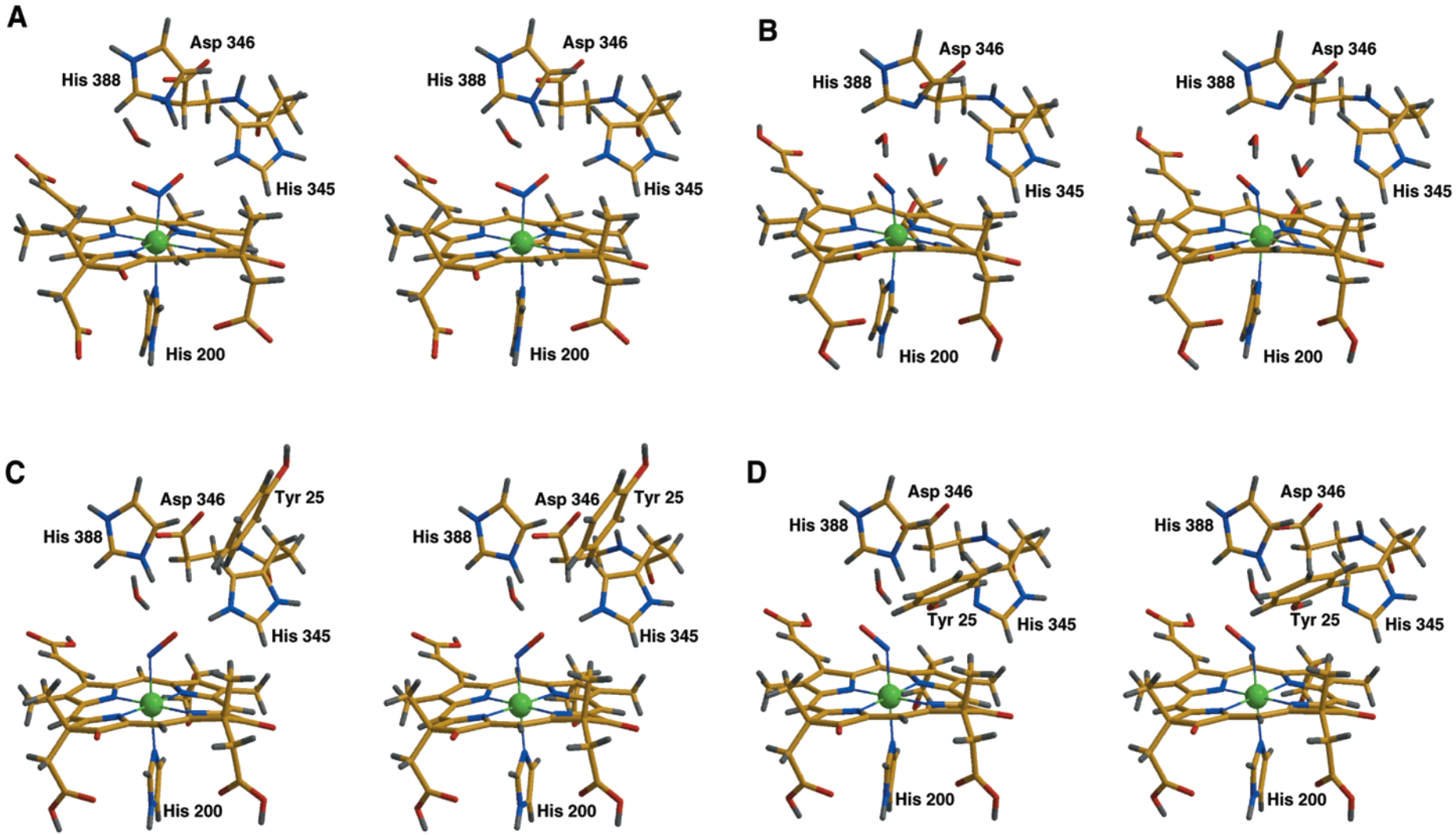

FIGURE 2: Stereoviews of the active site of cytochrome cd_1 from *P. pantotrophus* at various stages of nitrite reduction. (A) X-ray structure of the [Fe(II)-NO_2^-] complex [PDB entry 1AOQ (subunit A)]. (B) Computed structure of the [Fe(III)-NO] complex immediately after water release and valence isomerization. (C) X-ray structure of an [Fe(III)-NO] complex [PDB entry 1AOQ (subunit B)]. (D) X-ray structure of the [Fe(III)-NO] complex with the oxygen of Tyr25 at the position of the product water molecule [PDB entry 1AOM (subunit B)]. Quantum chemical calculations show that nitric oxide release is easiest from structure D (see the text), but it can also happen from structure B. Figures were drawn using the program Molscript (*31*) and rendered with Raster 3D (*32*).

Table 2: Energy of the Unliganded Active Site as a Function of the Protonation States of His345 and His388 at Different Oxidation States of the d_1 Heme[a]

	$E_{tot} + E_{prot}$ (au) ab initio	ΔE (kcal/mol) ab initio	$E_{binding-NO_2^-}$ (kcal/mol) DISCOVER
Reduced d_1 Heme in 1AOF (*3*)			
His345 and His388	−4007.0743	0.0	0.0
His345 and His388$^+$	−4007.2046	−81.8	−62.9
His345$^+$ and His388	−4007.1739	−62.5	−38.2
His345$^+$ and His388$^+$	−4007.2326	−99.3	−40.0
Oxidized d_1 Heme in 1AOF (hypthetical structure)			
His345 and His388	−4007.0909	0.0	
His345 and His388$^+$	−4007.1333	−26.6	
His345$^+$ and His388	−4007.0943	−2.1	
His345$^+$ and His388$^+$	−4007.0814	6.0	

[a] The model used in these calculations is derived from the structure of the reduced enzyme [1AOF (*3*)] and contains all atoms of the d_1 heme, the axial histidine ligand (His200), residues His345, His388, and Asp346 above the heme plane, and two water molecules. E_{tot} is the total energy of the model, and E_{prot} is the contribution that accounts for the protonation energy. This term is computed as the difference in the total energy between the isolated protonated and unprotonated histidines (−0.5600 au, where 1 au = 627.502 kcal), and allows for a comparison between the models that differ in the number of protons on the two histidines. ΔE is the difference between the energy reported in column 1 and the same energy computed for the structure with neutral histidines as a reference. ΔE (DISCOVER) shows results when solvation and screening by the whole protein and its ordered solvent environment are taken into account through molecular mechanics calculations on an extended model (for details, see Methods). Due to a lack of an appropriate force field for Fe(III), ΔE (DISCOVER) values for the complex on an oxidized d_1 heme were not computed.

Table 3: Effect of the Protonation State of His345 and His388 on the Energy of the Enzyme−Nitrite Complex[a]

	$E_{tot} + E_{prot}$ (au) ab initio	ΔE (kcal/mol) ab initio	$E_{binding-NO_2^-}$ (kcal/mol) DISCOVER
Nitrite Structure **1** (60 s in nitrite, 1AOM)			
His345 and His388	−3160.0537	0.0	73.2
His345$^+$ and His388	−3160.2558	−129.2	11.97
His345 and His388$^+$	−3160.2596	−126.8	8.91
His345$^+$ and His388$^+$	−3160.3899	−211.0	−52.4
Nitrite Structure **2** (180 s in nitrite, 1AOQ)			
His345 and His388	−3160.0316	0.0	
His345$^+$ and His388	−3160.2307	−76.3	
His345 and His388$^+$	−3160.2279	−78.0	
His345$^+$ and His388$^+$	−3160.3523	−201.2	

[a] Two very similar models were used in these calculations derived from structures (*3*) 1AOM (subunit A, 60 s in nitrite) and 1AOQ (subunit A, 180 s in nitrite). The latter model is shown in Figure 2A. For other details, see the footnote of Table 2. $E_{binding-NO_2^-}$ (DISCOVER) represents the binding energy of nitrite when solvation and screening by the whole protein and its ordered solvent environment ar taken into account (for details, see Methods); 1 au = 627.502 kcal.

The calculated position of this water molecule is similar to the position of the tyrosine oxygen in Figure 2D (shown schematically as structure **7** in Figure 1). We note that the vicinity of the two histidines and their charge state must affect the orientation and p*K* of bound ligands at this position. We also note that the three-dimensional arrangement of Asp346, His388, and the product water is similar to the arrangement of the Asp-His-Ser-OH catalytic triad of serine proteases.

Valence Isomerization on the d_1 Heme. Oxidation of the d_1 heme iron requires the transfer of an electron from the ferrous iron to the bound NO^+ cation. The resulting [Fe(III)-NO] complex (structure **5** in Figure 1) is isoelectronic with structure **4**. Ozawa et al. (*27*) showed on model compounds that the nitrosyl complex of the d_1 heme gives two diamagnetic species: the [Fe(II)-NO^+] and the [Fe(III)-NO] forms. The [Fe(II)-NO^+] form has also been observed by Fourier transform infrared spectroscopy in cytochrome cd_1 (*28*). Our calculations are in agreement with these observations. Structures **4** and **5** in Figure 1 represent these structures, respectively. Structure **5** can be generated from a hypothetical structure in which His345 and His388 are protonated, the heme iron is in the ferric state, the bound nitric oxide is uncharged, and a single oxygen atom with two negative charges is placed at the position of the tyrosine oxygen of structure **7**. Following proton migration and bond formation, the final structure in the stimulated annealing experiment gave structure **5**. Structure **4** can also be converted into structure **5**. Simulated annealing studies on the two isoelectronic species gave similar structural features with slightly different angles for the Fe−N−O bond (139.4° for structure **4** and 153.7° for structure **5**). The calculations also showed that the heme ring distortion from planarity was fairly small in both structures. Structure **5** in Figure 1 was more stable than structure **4** by about −10.9 kcal/mol.

In simple symmetrical model compounds of iron−protoporphyrin IX complexes, NO usually binds in a bent conformation to Fe(II) and in a linear manner to Fe(III). These binding modes may be distorted if the heme is not symmetrical or if the porphyrin ring is not continuously conjugated. Distal interactions in a protein molecule may also favor altered conformations. These factors influence NO geometries in the active site of cytochrome cd_1. The d_1 heme of cytochrome cd_1 is not continuously conjugated (*1*, *2*) and as a consequence, the four nitrogen ligands surrounding the iron have different electronic properties. This, together with steric, electrostatic, and hydrogen-bonding interactions between the bound NO and residues in the distal pocket of the active site (*3*) (Figures 1 and 2), affects the Fe−N−O geometry, and makes simple comparisons with model data difficult on symmetrical heme compounds. All geometry optimizations on NO bound to the d_1 heme ended up with bent Fe−N−O geometries in agreement with X-ray data (*3*) on NO−d_1 heme complexes.

Table 4 gives the energies and symmetries of frontier molecular orbitals in the [Fe(II)-NO^+] and [Fe(III)-NO] resonance forms, and compares them with the symmetries of frontier molecular orbitals in the [Fe(II)-$NO^\bullet$] radical. This latter complex can be formed by accident if nitric oxide binds to a reduced d_1 heme or if the heme becomes reduced before product release. The two strong bonds between nitric oxide and Fe(II) in the radical form are described by the two uppermost orbitals in column 1 of Table 4. The highest occupied molecular orbital (HOMO) is a bonding orbital describing the Fe(II)−oxygen back-donation. A singly occupied molecular orbital (SOMO), represented by Fe(II)(d_z)-_nitrogen(sp)_oxygen(sp), is the bonding orbital. The spin population is highest on the d_{z^2} orbital of the iron. The LUMO is a π-type orbital delocalized on the heme ring. Rearrangement of the positive charge in the [Fe(II)-NO^+] complex produces [Fe(III)-NO]. The stabilization of this latter form can be seen in the total energy gain and in the gain of stability of the HOMO in the [Fe(III)-NO] complex. The [Fe(III)-

Table 4: Energies (au) and Symmetries of Frontier Molecular Orbitals in Three Different Electronic States of the d_1 Heme−NO Complex in Cytochrome cd_1 Nitrite Reductase

[Fe(II)-NO•]			[Fe(II)-NO$^+$]			[Fe(III)-NO]		
LUMO	−0.1621	heme π	LUMO+1	−0.2574	Fe−N−O	LUMO+1	−0.2659	heme π
SOMO	−0.1727	Fe−N−O	LUMO	−0.2682	heme π	LUMO	−0.2871	Fe−N−O
HOMO	−0.2045	Fe → O	HOMO	−0.3191	heme π	HOMO	−0.3225	Fe ← O

Table 5: Changes in the Interaction Energy of Bound NO and in the Total Energy of the System as a Consequence of the Rotation of Nitric Oxide and the Binding of Tyr25 between His345 and His388[a]

	His345 and His388	His345$^+$ and His388	His345 and His388$^+$	His345$^+$ and His388$^+$
(1) NO between His345 and His388, and Tyr25 Not Present (structure **6** in Figure 1 with four water molecules)				
ΔE_{total} (ab initio)	0	23	−33	−6
ΔE_{NO} (ab initio)	−73	−80	−90	−85
$E_{binding-NO}$ (Docking)	34	7	7	−20
(2) NO Rotated Away from His345 and His388, and Tyr25 Not Present (structure **7** in Figure 1 without Tyr25)				
ΔE_{total} (ab initio)	0	−24	−29	−1
ΔE_{NO} (ab initio)	−40	−61	−45	−45
$E_{binding-NO}$ (Docking)	27	6	−3	−24
$\Delta E_{total(1)-(2)}$	−37	−36	−41	−43
(3) Tyr25-OH between His345 and His388 (structure **7** in Figure 1)				
ΔE_{total} (ab initio)	0	10	−31	33
ΔE_{NO} (ab initio)	−47	−55	−69	−49
$E_{binding-NO}$ (Docking)	19	−2	−11	−32
(4) Negatively Charged Tyr25-O$^-$ between His345 and His388 (structure **7** in Figure 1)				
ΔE_{total} (ab initio)	0	−69	−61	−55
ΔE_{NO} (ab initio)	−60	−60	−51	−70
$E_{binding-NO}$ (Docking)	40	19	10	−11

[a] Models used in these calculations are shown in Figure 2. ΔE_{total} represents the change in the total energy of the model (in kcal/mol) relative to the form where His345 and His388 are unprotonated. ΔE_{NO} represents the interaction energy (in kcal/mol) between NO and the resting ferric d_1 heme models. $\Delta E_{total(1)-(2)}$ is the difference in the total energies of forms 1 and 2. $E_{binding-NO}$ (DOCKING) represents the binding energy of nitric oxide when solvation and screening by the whole protein and its ordered solvent environment are taken into account (for details, see Methods).

NO] complex (structure **5** in Figure 1) has a π-type HOMO, similar to the radical form, but it is a weaker back-donating orbital for donation from the oxygen to the iron. As a result, NO is bent in the [Fe(III)-NO] complex. The HOMO of structure **4** (Figure 1) is a delocalized π-type orbital on the heme, which also includes the $2p_y$ and $2p_z$ orbitals of the oxygen atom of nitric oxide, indicating that the positive charge is delocalized from the oxygen to the iron. The lowest unoccupied molecular orbital (LUMO) of the [Fe(III)-NO] complex is located on the Fe−N═O atoms.

The results support the view that the first step in the oxidation on the d_1 heme is driven by proton transfer from His345 and His388 to bound nitrite. This is followed by bond breakage and the formation of a water molecule. Valence isomerization in the resulting [Fe(II)-NO$^+$] complex gives [Fe(III)-NO].

Release of Nitric Oxide from the d_1 Heme. Fülöp et al. (*1*) suggested that NO release may be assisted by Tyr25, and proposed that in this process Tyr25 rebinds to the d_1 heme iron during the last step of the catalytic cycle. This proposal was based on the X-ray structure of the resting enzyme [structure **1** in Figure 1, the first structure for a cytochrome cd_1 (*1*)] and on the different binding propensities for binding of nitrogen and oxygen ligands to the oxidized and reduced heme iron (*29*, *30*). We calculated the interaction energy of the ferric d_1 heme for interaction with either nitric oxide or Tyr25 bound to the heme iron. The results confirm that the tyrosinate ligand binds much stronger (interaction energy of −159 kcal/mol) than nitric oxide (interaction energy of −80 kcal/mol) when the heme iron is in the ferric state. With a ferrous iron in the d_1 heme, the order reverses and the binding of nitric oxide becomes stronger (interaction energy of −147 kcal/mol) than the binding of Tyr25 (interaction energy of −90 kcal/mol).

Williams speculated (*3*, *21*) that under steady-state conditions the enzyme does not necessarily have to return to the fully oxidized form (structure **1** in Figure 1) to release NO, although it did so in the crystal in her experiments after the supply of nitrite and electrons had been exhausted (*3*). Recent experimental results on other cytochromes cd_1 (*13*, *14*, *24*) seem to support this speculation.

Release of bound nitric oxide from the heme iron is possible from structures **5**−**7** in Figure 1. Here we investigate stereoelectronic factors affecting the stability of nitric oxide bound to ferric d_1 heme in the active site of cytochrome cd_1 from *P. pantotrophus*. Figure 2B shows the stereomodel of the product complex (structure **5** in Figure 1), while Table 5 shows the energy of product complexes as a function of the protonation state of His345 and His388.

X-ray data available for two product complexes (structures **6** and **7** in Figure 1) show nitric oxide bound to the ferric heme in two orientations (Figure 2C,D). The structure of the d_1 heme in these complexes can be superimposed well (rmsd of 0.12 Å), suggesting that the oxidation state of the iron is the same. In structure **6** in Figure 1 (see also Figure 2C), nitric oxide points toward the histidines and the oxygen atom of nitric oxide takes up the position of the product water molecule. In the other X-ray structure (structure **7**; see also Figure 2D), the oxygen of Tyr25 occupies this position and nitric oxide is rotated around the Fe−N bond. A small horizontal displacement of the histidines in these complexes makes a negligible contribution to the overall thermodynamic

stability of the complex (−0.92 kcal/mol). However, the rotation of nitric oxide from its position in Figure 2B to the position in Figure 2C increases the stability of the complex in Figure 2C by −37 kcal/mol (Table 5), making the complex in Figure 2C (structure **6** in Figure 1) an unlikely structure for easy nitric oxide release. Results of these ab initio calculations suggest that nitric oxide is most likely to be released when both histidines are unprotonated in the structure in Figure 2B. This arrangement corresponds to the model of the first formed product complex (structure **5**) in Figure 1.

Protonation of His345 and/or His388 increases the stability of the enzyme−NO complex via the formation of H-bonds between nitric oxide and the histidines. In such a complex, the oxygen of NO replaces the product water between His345 and His388 (structure **6** in Figure 1, Figure 2C), and NO release becomes more difficult (Table 5). Protonation of His345 and/or His388 can happen via Asp346 and via a chain of solvent molecules observed in the structure. Protonation of His388 gives rise to a very stable complex (Table 5). The difference in the energies of the two singly protonated states (see also Tables 1 and 4) suggests a double-step mechanism for the reprotonation of the histidines (His388 first, followed by His345).

Hydrogen bonds between nitric oxide and His345 and/or His388 stabilize a bent Fe−N−O conformation, and external ligands that are capable of entering into hydrogen bonding interactions with these histidines may alter the Fe−N−O geometry. Tyr25 is one such ligand. Tyr25 approaches the d_1 heme site as a consequence of a large rearrangement in the *c* haem domain (*3*). This rearrangement is associated with a change in the oxidation state of the hemes. Binding of Tyr25 between His345 and His388 in Figure 2D breaks hydrogen bonds to NO, and creates an unfavorable NO orientation (Figure 2B). Rotation of nitric oxide in the complex is the result of steric effects, and is driven by the energy gain in the system due to the formation of strong hydrogen bonds and ionic interactions between the incoming tyrosine or tyrosinate and the two histidines. We also note that the four nitrogen ligands of the iron in the plane of the d_1 heme are not equivalent.

External ligands capable of binding between His345 and His388 will create a similarly unfavorable NO orientation as Tyr25 in structure **7** (Figure 1), and could assist in lowering the interaction energy of nitric oxide within the complex in a similar fashion. Known ligands that can bind to the same position as the tyrosine oxygen between His345 and His388 are the product water molecule (structure **5** in Figure 1) and one of the oxygens of the incoming nitrite ion (nitrite accepts hydrogen bonds from His388 and/or His345 in the enzyme−nitrite complex; see structure **3** in Figure 1). The orientation, p*K*, and stability of ligands capable of binding between His345 and His388 depend on the protonation states of the histidines. These findings suggest that known cytochromes cd_1 may actually use the same mechanisms for NO release but may employ different ligands (or a range of ligands) to create an unfavorable nitric oxide orientation.

Table 5 also lists the docking energies of nitric oxide when solvation and screening by the whole protein and its ordered solvent environment are taken into account (for details, see Methods). The results indicate that the doubly protonated form ($His345^+$ and $His388^+$) strongly attracts the bound nitric oxide moiety. The presence of charged Tyr25 in the pocket lowers this attractive energy. The singly protonated forms are not equally stable, except for structure **6** in Figure 1. The nonprotonated state produces a repulsive energy for NO binding between His345 and His388 in all cases, when the effect of charges elsewhere in the protein and the effect of screening and solvation by the protein and its surrounding medium are included in the model. The ab initio and molecular mechanics calculations agree for structure **7**. Both types of calculations show that NO release is easiest from the active site when His345 and His388 are unprotonated, except for case 4 of Table 5, where the ab initio results show slightly more destabilization for the form with His345 unprotonated and His388 protonated.

CONCLUSIONS

Reduction of nitrite to nitric oxide is the committed step in bacterial denitrification, and the reaction has certain environmental implications. Another aspect of nitrite reduction by cytochromes cd_1 is that nitric oxide is formed on a heme center, from where it must be released as a reaction product. Interest in the mechanism of nitric oxide release from a heme iron stems from its relevance to understanding the release of nitric oxide from heme-containing receptors (e.g., cGMP cyclase) in higher cells.

The main aim of this work was to clarify apparent disagreements in the mechanisms proposed for nitrite reduction by cytochromes cd_1. Quantum mechanical methods were used to understand electronic rearrangements in the reaction, and molecular mechanics methods were applied to account for environmental modulations. These methods (ab initio and molecular mechanics) produced different energies, and sometimes slightly different conclusions. However, the overall trend of the data points to the same interpretation. The results can be summarized as follows. (i) His345 and His388 are protonated in the active site of the unliganded reduced form of cytochrome cd_1 (structure **2** in Figure 1). (ii) Nitrite binds to this doubly protonated enzyme form. (iii) Nitrite reduction starts with proton transfer from the histidines to the bound nitrite ion. This process cleaves off a water molecule from the substrate and leaves an NO^+ cation on a still reduced d_1 heme. (iv) Electron transfer from the d_1 heme to the bound NO^+ cation creates the more stable [Fe(III)-NO] product complex. The orientation and stability of nitric oxide in this complex depend on possible hydrogen bonding interactions with His345 and His388 in the active site. (v) Release of nitric oxide from the d_1 heme can happen in more than one way. Delocalization is not continuous in the d_1 heme, and as a consequence, the four nitrogen ligands surrounding the iron in the heme plane are not equivalent. Ionic and hydrogen bonding interactions with His345 and/or His388 can stabilize and orient nucleophilic ligands above the heme plane. The oxygen of Tyr25, or another ligand capable of binding temporarily between His345 and His388, facilitates NO release by imposing an unfavorable orientation on NO in the active site. Comparison of the interaction energies of nitric oxide in structures in Figure 1 indicates that the most likely structure for NO release is structure **7**, followed by structures **5** and **6**, in this order. The total energy of these complexes and the interaction energy of nitric oxide within these complexes are influenced by the protonation

states of His345 and His388. The calculations suggest that a rebinding of the phenolate oxygen of Tyr25 to the iron of the d_1 heme may be bypassed in steady-state catalysis. Tyr25 does eventually rebind to the heme iron when the supply of electrons to the d_1 heme is low.

The results allow a description of the electronic mechanism of nitrite reduction in the active site of cytochrome cd_1. The findings are in agreement with experimental results, and offer a unification of proposals for the mechanism of nitrite reduction by cytochromes cd_1.

ACKNOWLEDGMENT

We thank Prof. S. Ferguson and Drs. M. Ek, V. Fülöp, and E. Steensma for discussions. We thank Dr. Chiara Carbonera for help in the molecular mechanics calculations.

REFERENCES

1. Fülöp, V., Moir, J. W., Ferguson, S. J., and Hajdu, J. (1995) *Cell 81*, 369−377.
2. Baker, S. C., Saunders, N. F., Willis, A. C., Ferguson, S. J., Hajdu, J., and Fülöp, V. (1997) *J. Mol. Biol. 269*, 440−455.
3. Williams, P. A., Fülöp, V., Garman, E. F., Saunders, N. F., Ferguson, S. J., and Hajdu, J. (1997) *Nature 389*, 406−412.
4. Hadfield, A., and Hajdu, J. (1993) *J. Appl. Crystallogr. 26*, 839−842.
5. Mozzarelli, A., and Rossi, G. L. (1996) *Annu. Rev. Biophys. Biomol. Struct. 25*, 343−365.
6. Edman, K., Nollert, P., Royant, A., Belrhali, H., Pebay-Peyroula, E., Hajdu, J., Neutze, R., and Landau, E. M. (1999) *Nature 401*, 822−826.
7. Wilmot, C. M., Hajdu, J., McPherson, M. J., Knowles, P. F., and Phillips, S. E. (1999) *Science 286*, 1724−1728.
8. Alefounder, P. R., and Ferguson, S. J. (1980) *Biochem. J. 192*, 231−240.
9. Zumft, W. G. (1997) *Microbiol. Mol. Biol. Rev. 61*, 533−616.
10. Ferguson, S. J. (1998) *Curr. Opin. Chem. Biol. 2*, 182−193.
11. Silvestrini, M. C., Tordi, M. G., Musci, G., and Brunori M. (1990) *J. Biol. Chem. 265*, 11783−11787.
12. Cheesman, M. R., Ferguson, S. J., Moir, J. W., Richardson, D. J., Zumft, W. G., and Thomson, A. J. (1997) *Biochemistry 36*, 16267−16276.
13. Nurizzo, D., Silvestrini, M. C., Mathieu, M., Cutruzzola, F., Bourgeois, D., Fülöp, V., Hajdu, J., Brunori, M., Tegoni, M., and Cambillau, C. (1997) *Structure 5*, 1157−1171.
14. Nurizzo, D., Cutruzzola, F., Arese, M., Bourgeois, D., Brunori, M., Cambillau, C., and Tegoni, M. (1998) *Biochemistry 37*, 13987−13996.
15. Fletcher, R. (1980) *Practical methods of Optimisation*, John Wiley & Sons, New York.
16. Kohn, W., and Sham, L. J. (1965) *Phys. Rev. 140A*, 1133.
17. Harris, J. (1985) *Phys. Rev. B31*, 1770.
18. Barth, v. U., and Hedin, L. (1972) *J. Phys. C: Solid State 5*, 2064−2070.
19. Kirkpatrick, S., Gelatt, C. D., and Vecchi, M. P. (1983) *Science 220*, 671−680.
20. Angelucci, L., Degioia, L., and Fantucci, P. (1993) *Gazz. Chim. Ital. 123*, 111−117.
21. Williams, P. A. (1996) Time-resolved structural studies on macromolecules, Thesis, Oxford University, Oxford, U.K.
22. Berks, B. C., Ferguson, S. J., Moir, J. W., and Richardson, D. J. (1995) *Biochim. Biophys. Acta 1232*, 97−173.
23. Kobayashi, K., Koppenhofer, A., Ferguson, S. J., and Tagawa, S. (1997) *Biochemistry 36*, 13611−13616.
24. Cutruzzola, F., Arese, M., Grasso, S., Bellelli, A., and Brunori, M. (1997) *FEBS Lett. 412*, 365−369.
25. Jungst, A., Braun, C., and Zumft, W. G. (1991) *Mol. Gen. Genet. 225*, 241−248.
26. Smith, G. B., and Tiedje, J. M. (1992) *Appl. Environ. Microbiol. 58*, 376−384.
27. Ozawa, S., Sakamoto, E., Ichikawa, T., Watanabe, Y., and Morishima, I. (1995) *Inorg. Chem. 34*, 6362−6370.
28. Wang, Y. N., and Averill, B. A. (1996) *J. Am. Chem. Soc. 118*, 3972−3973.
29. Pettigrew, G. W., and Moore, G. R. (1987) *Cytochromes c: Biological aspects*, Springer-Verlag, Berlin.
30. Moore, G. R., and Pettigrew, G. W. (1990) *Cytochromes c: Evolutionary, Structural and Physicochemical Aspects*, Springer-Verlag, Berlin.
31. Kraulis, P. J. (1991) *J. Appl. Crystallogr. 24*, 946−950.
32. Merrit, E. A., and Murphy, M. E. P. (1994) *Acta Crystallogr. D50*, 869−873.

BI000178Y